Phase Separation Oppositely Modulates G-quadruplex and i-Motif DNA Folding in the Nuclei of Living Cells

Brahmmi Patel, Cailin Hoang, Hyejin Yoo†, Caitlin M. Davis*

Department of Chemistry, Yale University, 225 Prospect Street, New Haven, Connecticut 06511-6712, United States

ABSTRACT: G-quadruplexes and i-motifs are non-canonical DNA structures that are thought to play an important role in the regulation of gene expression. Although these structures have been well studied in vitro, they are often characterized in non-physiological buffers intended to stabilize their structure. Therefore, additional work is necessary to understand how the cellular environment promotes their folding. Here we investigate the folding of the 15-mer thrombin-binding aptamer G-quadruplex (G4) and the designed 35-mer TAA(C_5TAA)$_4$ i-motif (iM) inside living osteosarcoma cells. We use fast relaxation imaging, which couples fluorescence microscopy with a laser-induced temperature jump, to quantify the stability and dynamics of FRET-labeled constructs. The melting temperature of G4 and iM inside cells are 44.9 ± 0.9 °C and 46.5 ± 0.6 °C, respectively. Compared to in vitro buffers, inside cells G4 is destabilized by ≈10 °C and iM is stabilized by ≈20 °C. These in-cell stabilities cannot be replicated by simple buffers that account for macromolecular crowding or non-specific interactions in the nuclear environment. Instead, specific interactions with nuclear proteins produce the observed in-cell stability trends. Furthermore, our results reveal that charge-driven condensation regulates the in-cell folding kinetics of both G4 and iM. Our work suggests that the kinetics of i-motif and G-quadruplex DNA are carefully tuned by phase separation to fit the seconds-to-minutes timescales of key regulatory processes inside cells. Taken together, our findings underscore the importance of studying the folding of DNA structures under near-physiological conditions to their mechanistic understanding as well as for the development of DNA-targeted drugs.

INTRODUCTION

In addition to the canonical B-form double helix, DNA is capable of adopting alternative inter- and intra-molecular secondary structure conformations, including guanine-quadruplex (G-quadruplex) and intercalated motif (i-motif) structures.[1,2] G-quadruplexes and i-motifs are found on complementary guanine-rich and cytosine-rich stretches of the genome, respectively. G-quadruplexes are formed by stacked coplanar guanine tetrads that are stabilized by monovalent cations, such as K^+ and Na^+. i-motifs are assembled from four parallel cytosine-rich strands held together by hemi-protonated intercalated cytosine (C:C+) base pairs. The topology and dynamic nature of these DNA scaffolds make them useful in designing nanostructures, hydrogels, pH sensors, DNA motors, and nanomaterials.[3–8] Additionally, the promoter and telomeric regions of several oncogenes are enriched in guanine/cytosine tracts that have the potential to form G-quadruplexes and i-motifs, making them novel drug targets.[9–13] Indeed, stabilization of G-quadruplexes and i-motifs suppresses transcriptional activation and telomerase activity in multiple oncogenes.[14–20]

The use of G-quadruplexes and i-motifs in biomedical, pharmacological, and nanotechnological applications is heavily dependent on the stability of these structures. Their stability depends on a number of factors, including the number of bases forming the motifs, the length and composition of the loops between them, and the local environment (e.g. ionic strength, pH, molecular crowding, and temperature).[21,22] Their apparent stabilities under physiological conditions in vitro have led to skepticism towards their biological relevance. G-quadruplexes tend to have thermal stabilities far above physiological (37 °C) that are further stabilized by environmental conditions anticipated in cells, such as high ionic strength and macromolecular crowding.[21] Conversely, i-motifs do not fold at neutral pH in dilute aqueous solution. Hemi-protonation of cytosine tracts, often induced by non-physiological slightly-acidic pHs, is critical for the formation of the i-motif.[23–26] Additionally, cellular conditions such as macromolecular crowding and divalent cations promote i-motif folding at neutral pH.[27] Due to these observations, their existence in vivo remained speculative until recently when the presence of both G-quadruplexes and i-motifs inside living cells was confirmed.[28–31] However, the folding of G-quadruplexes and i-motifs in vitro has not been quantitatively compared to living cells. Understanding their stabilities in the native cellular context is critical for the advancement of targeted therapies and drug delivery systems in living cells and has far-reaching implications in the biomedical use of these structures.

Here, we measure the stability and dynamics of a FRET-labeled G-quadruplex and i-motif in living cells. To interpret our in-cell measurements we compare with analogous in vitro experiments in dilute buffer and cellular mimetics. We selected the thrombin-binding aptamer (TBA, Figure 1A) as our G-quadruplex model since it is well-characterized in

vitro with a near physiological thermal stability, 52 °C.[32–34] TBA has potential for many biomedical applications due to its inhibition of thrombin protease, the key enzyme in coagulation.[35] Due to their apparent instability, we did not use a naturally occurring i-motif; instead, we designed a thermally stable i-motif based on $(C_5TAA)_4$ repeat sequences (Figure 1B).[36,37] To quantify thermodynamics and kinetics in vitro and in living cells, we used Fast Relaxation Imaging (FReI), which combines fluorescence microscopy of FRET labeled biomolecules with laser-induced temperature jumps. In-cell FReI has been previously used to study folding of proteins and RNA as well as to quantify binding of proteins and nucleic acids.[38–41]

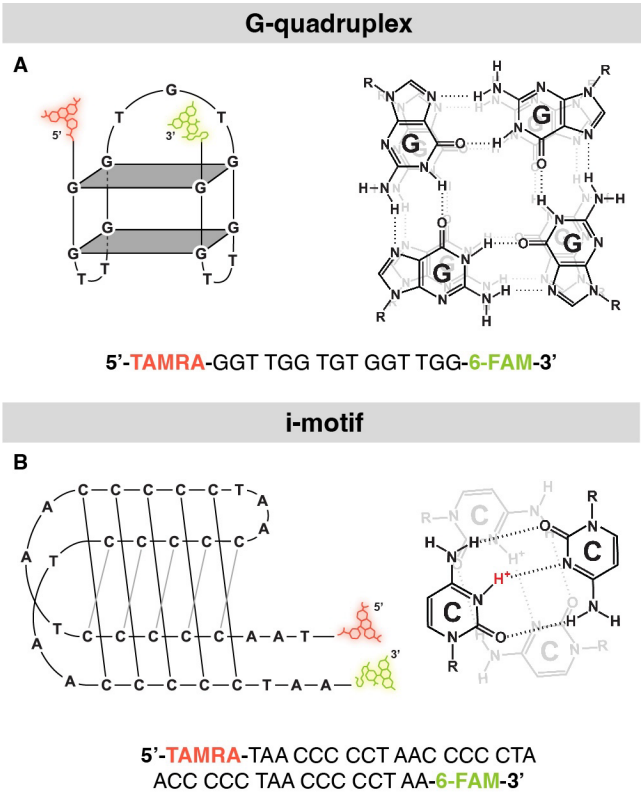

Figure 1. Cartoon of the secondary structure (left), chemical structure (right), and oligonucleotide sequence (bottom) of the FRET-labeled **(A)** anti-parallel 15-mer thrombin binding aptamer G-quadruplex DNA and **(B)** $(C_5TAA)_4$ i-motif DNA. Image generated in PowerPoint and Adobe Illustrator.

Using our FRET-based approach, we quantify the in vitro and in-cell stability and kinetics of both the FRET-labeled TBA G-quadruplex (G4) and FRET-labeled $(C_5TAA)_4$ i-motif (iM). While G4 is destabilized by ≈10 °C inside cells compared to in vitro, iM is stabilized by nearly ≈20 °C. These observations cannot be explained by macromolecular crowding or non-specific chemical interactions. Instead, we find that there are specific chemical interactions with proteins inside the cell nuclei which are responsible for the opposing effects on the stability of G4 and iM. The folding kinetics of G4 and iM are also oppositely affected: inside cells G4 folding is slowed while iM folding is sped. We find that the kinetics of G4 and iM inside cells are primarily governed by phase separation triggered by interactions with positively charged species in the nuclear environment. Taken together, our work emphasizes the importance of studying non-canonical DNA in native-like environment, especially for biomedical applications where the effectiveness of therapies relies on targeting the correct ensemble of states.

MATERIALS AND METHODS

DNA Oligonucleotides. TBA (5' – GGT TGG TGT GGT TGG – 3') and $(C_5TAA)_4$ (5' – TAA CCC CCT AAC CCC CTA ACC CCC TAA CCC CCT AA – 3') were purchased from Integrated DNA Technologies (IDT, Coralville, IA). To enable direct comparison between in vitro and in-cell measurements, the DNA were FRET-labeled (IDT) at the 5' and 3' ends with TAMRA (NHS ester) and 6-FAM (Fluorescein), respectively. Table S1 contains a complete list of oligos used in the study. Stock solutions of oligos were prepared at 100 µM in UltraPure DNase/RNase-Free Distilled Water (ThermoFisher Scientific, Waltham, MA) and stored at -20 °C.

Buffer Preparation. Polyethylene glycol 10,000 (PEG10k, Sigma-Aldrich, St. Louis, MO) was dissolved at 100-400 mg/ml in filtered potassium phosphate buffer (10 mM potassium phosphate, 200 mM KCl, 1 mM K_2EDTA, pH 7.0) and rocked overnight. To ensure that PEG was completely dissolved, the solution was heated to 55 °C for 20 minutes and cooled to room temperature prior to use.

Other buffers are commercially available. Nuclear Extraction Reagent (NER, ThermoFisher Scientific) was diluted to the desired concentration in potassium phosphate buffer. DPBS (Gibco, Grand Island, NY) was diluted from the manufacturer's 10X stock to 1X in distilled water, pH adjusted to 7.0 and filtered prior to use. Salmon sperm DNA (ssDNA, ThermoFisher Scientific) was dialyzed overnight at room temperature in phosphate buffer (10 mM potassium phosphate, 200 mM KCl, 1 mM K_2EDTA, pH 7.0). A mixture of 10 mg/ml BSA (Sigma), 37.5 %v/v NER, 2.5 mg/ml ssDNA, and 150 mg/ml PEG10k in 10 mM phosphate buffer pH 7 was prepared from buffer stocks.

Prior to in vitro analysis, the oligo stock was diluted to the final working concentration in the desired experimental buffer and annealed in a Nexus Gradient Thermal Cycler (Eppendorf, Hamburg, Germany); following established protocols,[42] each sample was heated to 90 °C for 5 minutes before slow cooling to 4 °C at a rate of 0.5 °C/min. To avoid refolding ssDNA, oligo stocks were annealed in the thermocycler prior to dilution in buffers containing ssDNA.

Nuclear Cell Lysate Preparation. Cultured human bone osteosarcoma epithelial cells, U-2 OS (ATCC HTB-96, Manassas, VA), were grown to ≈80% confluency in a T175 cell culture flask (ThermoFisher, Scientific). DMEM (Corning, Corning, NY) + 10% fetal bovine serum (FBS, ThermoFisher Scientific) + 1% penicillin-streptomycin (P/S, Corning) media was aspirated, and cells were washed with 10 ml of 1X PBS buffer (ThermoFisher Scientific). PBS was aspirated and 1 ml of pre-warmed trypsin-EDTA (Corning)

was added. The flask was placed in a 37 °C incubator for 5 minutes and then resuspended in 10 ml of 4 °C PBS buffer to inactivate the trypsin. The cell suspension was spun down at 500 xg for 3 minutes. The pellet was rinsed with 10 ml of PBS buffer before being spun down again at 500 xg for 3 minutes. Nuclear cell lysate was prepared using the NE-PER™ Nuclear and Cytoplasmic Extraction Reagents Kit (ThermoFisher Scientific) and following the manufacturer's protocol. The nuclear cell lysate was dialyzed overnight in phosphate buffer (10 mM potassium phosphate, 200 mM KCl, 1 mM K_2EDTA, pH 7.0) at room temperature in a Slide-A-Lyzer™ 3.5K MWCO MINI Dialysis Device (ThermoFisher Scientific). The concentration of the nuclear lysate was quantified using a Pierce™ Bradford Protein Assay Kit (ThermoFisher Scientific) and used immediately. To avoid denaturing proteins in the lysate, oligo stocks were annealed in the thermocycler prior to dilution in nuclear cell lysate.

Turbidity Assay. Turbidity was assessed in solutions with increasing concentrations of DNA and 0.1 mg/ml unlabeled poly-L-lysine (PLL). 5 μM of pre-annealed unlabeled or FRET-labeled DNA was diluted to the desired final concentration in a solution containing 0.1 mg/ml unlabeled PLL (25988-63-0, Electron Microscopy Sciences) or FITC-labeled PLL (P3069, Sigma) in phosphate buffer (10 mM potassium phosphate, 200 mM KCl, 1 mM K_2EDTA pH 7.0) and incubated for 30 minutes at RT. After incubation, the absorbance at 400 nm of the unlabeled mixture was measured using a Nanodrop One spectrophotometer (Thermo Scientific). An average of three readouts was recorded. Fluorescent samples were used for complementary fluorescence imaging.

Fluorescence Spectroscopy. Steady-state FRET measurements were performed on a FP-8500 Spectrofluorometer (JASCO, Easton, MD) equipped with an automatic 4-position Peltier cell changer with temperature controller (PCT-818, JASCO). Experiments were performed at 0.50 μM in a 10 mm pathlength microcuvette (16.160F-Q-10/Z15, Starna Cells, Atascadero, CA). 6-FAM was excited at 480 nm with a 5 nm slit width, and fluorescence was monitored from 475 to 700 nm in 1 nm intervals. Thermal denaturation was performed from 10 to 79 °C in 3 °C intervals with an equilibration time of 3 minutes prior to acquisition. Samples were covered with mineral oil to prevent evaporation.

DNA Microinjection and Transfection. DNA was introduced into U-2 OS cells via microinjection or transfection. U-2 OS cells were cultured and grown to 80% confluency on coverslips (No. 1.5, MatTekCorp., Ashland, MA) in DMEM containing 1% P/S and 10% FBS. For microinjection, cells were rinsed with PBS and resuspended in Fluorobrite (Gibco) supplemented with 10% FBS (FemtoJet 4i, Eppendorf, Enfield, CT). The 100-200 μM stock of FRET-labeled oligos was annealed in a thermocycler before microinjection into cells. Alternatively, cells were transfected with a 1:3 μg:μl ratio of DNA plasmid to JetPRIME® Transfection Reagent (Polyplus, Illkirch, FR) and incubated at 37 °C for 16 hours before imaging. Microinjected or transfected cells were rinsed with PBS, resuspended in Fluorobrite supplemented with 10% FBS, and mounted onto a microscope slide (1 mm, VWR, Radnor, PA) with a 120 μm spacer (GraceBioLabs, Bend, OR) for FReI imaging.

FReI. The FReI setup has been described previously.[40] Briefly, a 1950 nm infrared laser (AdValue Phototonics, Tucson, AZ) introduces a rapid step-function shaped temperature perturbation to the sample after which the sample is given 10-180 s to equilibrate. The temperature change is determined using the temperature-dependence of the quantum yield of mCherry.[43]

Fluorescence from the laser-heated field of view is imaged through an objective lens (EC Plan-Neofluar 63X/0.85, Zeiss, Oberkochen, Germany) onto a CMOS camera (Moment, Teledyne Photometrics, Tucson, AZ). To excite the 6-FAM donor fluorophore, a white LED (X-Cite mini+, Excelitas, Waltham, MA) is passed through an ET480/40X bandpass filter (Chroma, Bellows Fall, VT) and then reflected onto the sample by a FF509-FDi 01 dichroic mirror (Semrock, West Henrietta, NY). Fluorescence emission is passed through a long-pass filter (ET510lp, Chroma) and split into red and green light by an Optosplit III emission image splitter (Cairn Research, Kent, UK) containing a dichroic mirror (FF560-FDi 01, Semrock). Images are collected at a frame rate of 5 fps for in-cell measurements and 1-40 fps for in vitro measurements.

Analysis of Thermodynamic Data. All thermal denaturation curves were fit to a two-state equilibrium model[38]:

$$S(T) = \frac{[\alpha_D+\beta_D(T)]+[\alpha_N+\beta_N(T)]e^{-\frac{\Delta G}{RT}}}{(1+e^{-\frac{\Delta G}{RT}})}, \text{(E1)}$$

where α_N and α_D are the signals from the native (N) and denatured (D) states, respectively, and β_N and β_D are the slopes of the baselines from the native and denatured state, respectively. R is the ideal gas constant and ΔG is the free energy of unfolding (N to D) and can be approximated as a linear function of temperature: $\Delta G \approx \Delta G_1(T - T_m)$.[38]

Analysis of Kinetic Data. The kinetics were plotted as the donor/acceptor ratio (D/A) versus time and fit to a double exponential function:

$$S(t) = y_0 + A_1 e^{\{\frac{-(t-t_0)}{\tau_1}\}} + A_2 e^{\{(\frac{-(t-t_0)}{\tau_2})^{\beta}\}}, \text{(E2)}$$

where the signal, S, as a function of time, t, is described by the sum of two exponential functions with pre-exponential factors, A_1 and A_2, and relaxation lifetimes, τ_1 and τ_2. The first exponential accounts for the instrument response, relaxation lifetimes of the fluorophores, and fast unresolved dynamics of the system. The second stretched exponential describes the folding/unfolding dynamics of the system following the temperature jump where τ_2 is the relaxation lifetime. The stretched exponential factor, β, allows for deviations from a simple two-state folding mechanism.[43,44]

RESULTS AND DISCUSSION

G4 and iM are folded near physiological temperature and pH in crowded environments. Before investigating the stability of G4 and iM inside cells, we performed equilibrium circular dichroism measurements in vitro on labeled and unlabeled constructs to validate that FRET-labeling minimally perturbs their structure and thermal stability (SI Methods and Discussion, Figure S1). FRET has been used previously to study the in vitro folding of G4 as well as other G-quadruplexes and i-motif DNA.[45–48] A donor (D) and acceptor (A) fluorophore are covalently attached to the 5' and 3' ends of the DNA, and FRET reports on the end-to-end distance of the DNA. A low donor/acceptor (D/A) ratio occurs when there is high FRET, where the fluorophores are close together and energy is transferred non-radiatively from the excited donor fluorophore to the acceptor fluorophore, such as in the folded state. A high D/A ratio indicates that the fluorophores are farther apart, such as in the unfolded state, reducing the efficiency of the energy transfer.

To predict the nuclear behaviors of G4 and iM, we investigated their folding in vitro near the physiological pH and macromolecular crowding concentration present in the cell (pH 7.0 and 200 mg/ml PEG10k).[49,50] The FRET detected temperature-induced denaturation of G4 and iM is shown in Figure S2. The in vitro melting temperatures of G4 and iM are 58.9 ± 0.2 °C and 28.6 ± 0.7 °C, respectively (Figure 2). Ideal constructs for in cell folding studies will have stabilities at near-physiological temperatures that are not harmful to the cells. The in vitro stability of G4 is at the temperature limit of what has been previously measured in cells; infrared heating has been used to study folding as well as heat-shock response and gene induction up to 60 °C.[40,51] Therefore, the in-cell stability was measured before making any destabilizing mutations to the sequence.

G4 is destabilized whereas iM is stabilized by the nuclear environment. FReI combines fluorescence microscopy of FRET labeled biomolecules with small mid-IR laser-induced temperature jumps to thermally perturb the folding equilibrium. Thermal denaturation induced by the laser is monitored by changes in the donor and acceptor channels, and the stability is reported using the D/A ratio after the sample has time to fully equilibrate to the higher temperature. This approach is well established to study the folding of proteins and nucleic acids inside living cells with high spatio-temporal resolution.[39,40,52–56] Figure 2 shows representative FReI melting curves for G4 and iM in the nucleus of living cells.

Inside the nucleus, G4 has an average melting temperature of 44.9 ± 0.9 °C (n=36) (Figure 2A, Table S2) compared to 58.9 ± 0.2 °C predicted by the in vitro FRET melts. The stability of G-quadruplexes is highly dependent on the identity of chemical species in solution.[57] For example, G-quadruplexes are more stable in buffers containing potassium ions than buffers containing sodium ions.[58] Indeed, at neutral pH, G4 is 25 °C less stable in DPBS, which is predominantly Na^+, than in potassium phosphate buffer (SI Discussion, Figure S3A, Table S3). Thus, the 14 °C decrease in stability is likely due to destabilizing chemical interactions with solutes, small molecules, and macromolecules in the nucleus of the cell.

Whereas G4 is destabilized inside cells, iM is significantly stabilized. iM has an average melting temperature of 46.5 ± 0.6 °C (n=60) inside the nucleus (Figure 2B, Table S4) compared to 28.6 ± 0.7 °C predicted by in vitro fluorescence melts. The 18 °C stabilization in the nucleus of cells could arise from macromolecular crowding, which is always stabilizing, or chemical interactions, which can be stabilizing or destabilizing. Like G4, iM is destabilized in sodium buffers when compared to phosphate buffers (Figure S3B, Table S5). Therefore, further experiments are necessary to determine the origin of differences in the stability of G4 and iM in the nucleus of cells.

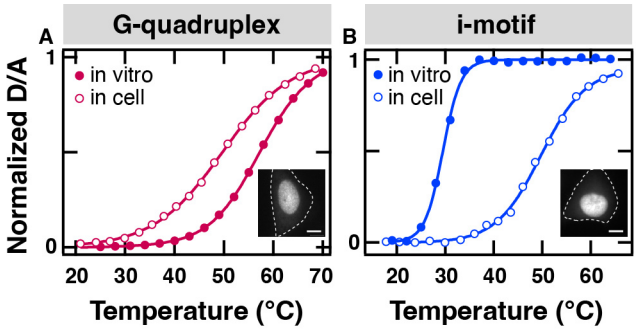

Figure 2. Representative equilibrium temperature denaturation of **(A)** G4 and **(B)** iM monitored by fluorescence spectroscopy in vitro and FReI microscopy in the nucleus of U-2 OS cells. In vitro experiments were conducted in 200 mg/ml PEG10k (10 mM potassium phosphate, 200 mM KCl, 1 mM K_2EDTA, pH 7.0). The temperature dependent D/A ratios are fit (continuous line) to a two-state equilibrium model (Equation 1) and normalized to correct for pre- and post- transition baselines. Inset: Representative U-2 OS cells microinjected with FRET-labeled oligo that is localized to the nucleus. Cell outlined by white dashed line. Scale bar is 5 μm.

Nuclear measurements cannot be explained by macromolecular crowding alone. In cell measurements demonstrate that our near physiological buffer (pH 7.0 and 200 mg/ml PEG10k) is insufficient to replicate the nuclear environment. The total cytosolic concentrations of macromolecules in eukaryotic cells range from 10% to 40% w/v,[59] and the nuclear and cytosolic concentrations of macromolecules in U-2 OS cells are similar.[60] Therefore, to better understand the role that macromolecular crowding in the nucleus plays on folding of G4 and iM, their stabilities were measured in the presence of PEG10k between 0 and 300 mg/ml (Table 1, Figure S4). Higher concentrations of PEG10k were not tested due to lack of PEG solubility above 300 mg/ml. Macromolecular crowding theory predicts that the excluded volume induced by large macromolecules will result in entropic destabilization of extended or unfolded conformations, resulting in more energetically favorable compact, folded

states.[61] Indeed, the thermal stability of both oligos increased with increasing concentrations of PEG10k.

An increase in PEG10k concentration from 0 to 300 mg/ml yields an ≈9 °C increase in the stability of G4 (Table 1). This is consistent with prior investigations of unlabeled G4 that found macromolecular crowding induced by PEG results in thermal stabilization by the reduction of water activity.[62] The nuclear melting temperature is ≈14 °C lower than the melting temperature observed in vitro at near physiological crowding concentrations, 200 mg/ml PEG10k. Therefore, macromolecular crowding must not be the only effect (or dominating effect) modulating the stability of G4 inside cells. We hypothesize that chemical interactions must offset the stabilizing effect of macromolecular crowding on G4.

Macromolecular crowding alone also cannot explain the ≈19°C increase in iM stability observed in the nucleus of cells. Whereas a PEG titration from 0 to 300 mg/ml yields a ≈9°C increase in the stability of G4, it induces only a ≈2 °C stabilization of iM (Table 1). Our results match previous work on the c-MYC i-motif which found that 200 mg/ml PEG with sizes between 200 and 4K induce only a 1-2 °C stabilization at neutral pH.[63] That study showed that the same concentrations of PEG are more stabilizing at lower, non-physiological pHs. i-motifs are stabilized by base pairing between two cytosines, and optimal stability is achieved when one of the cytosines is protonated enabling three hydrogen bonds to form between the pair (Figure 1B).[64] Thus, at physiological pH, the presence of PEG only modestly increases the stability of iM compared to dilute buffer conditions (Table 1, Figure S4B). While steric crowding effects likely contribute to the stabilization of iM inside the nucleus, there must be other interactions that contribute to the large ≈19 °C stabilization observed inside cells.

Table 1. Melting temperatures (T_m) extracted from temperature-dependent FRET measurements of G4 and iM in increasing concentrations of PEG10k (10 mM potassium phosphate, 200 mM KCl, 1 mM K_2EDTA, pH 7.0). Error reflects the standard error of three replicates.

[PEG10k] (mg/ml)	G-quadruplex T_m (°C)	i-motif T_m (°C)
0	54.6 ± 0.2	27.5 ± 0.3
100	56.0 ± 0.2	28.5 ± 0.7
200	58.9 ± 0.2	28.6 ± 0.7
300	63.6 ± 0.2	29.7 ± 0.8

Nonspecific chemical interactions can be stabilizing or destabilizing, but no single effect replicates the nuclear stability trends of both G4 and iM. To isolate the effects of non-specific chemical interactions on G4 and iM, we measured their stabilities in vitro in buffers that mimic different cellular chemical interactions. We consider the effects of factors including the ionic strength, chemical composition of the nucleus, and the coexistence of nuclear DNA and proteins (Table S3, Table S5). All in vitro measurements were performed in 10 mM potassium phosphate, 200 mM KCl, 1 mM K_2EDTA, pH 7.0 to closely mimic the ionic strength and ionic composition of cells.[65]

Whereas macromolecular crowding by PEG (purple) induces compaction of both DNAs compared to phosphate buffer alone (blue), chemical interactions have differential effects on G4 and iM (Figure 3). Nonspecific chemical interactions in the nuclei are mimicked in vitro by small molecules, NER (green), and dilute solutions of macromolecules, ssDNA (orange) and BSA (magenta). The D/A at the beginning and end of the thermal melt reports on the end-to-end distance and structure of the folded and unfolded state, respectively. Although PEG has a larger effect on iM than G4, in both cases the initial and final D/A values are smaller (Figure 3), indicating that in crowded conditions the DNA accesses more compacted folded and unfolded states. Mimics of chemical composition of the nucleus on G4 are all destabilizing and result in expanded folded states of G4, with some variability in the effect on the unfolded state (Figure 3A). Similarly to G4, small molecules have the smallest effect on the structure of iM (Figure 3, green). Conversely from G4, chemical interactions with macromolecules promote more compacted folded and slightly expanded unfolded states of iM (Figure 3B). Although a melting temperature can be extracted from iM measurements made in potassium phosphate alone (Figure 3B, Figure S4B), the small ΔD/A value with increasing temperature supports CD measurements that show iM is predominantly disordered (Figure S1C). Thus, chemical interactions are an important regulator of G4 and iM structure and stability.

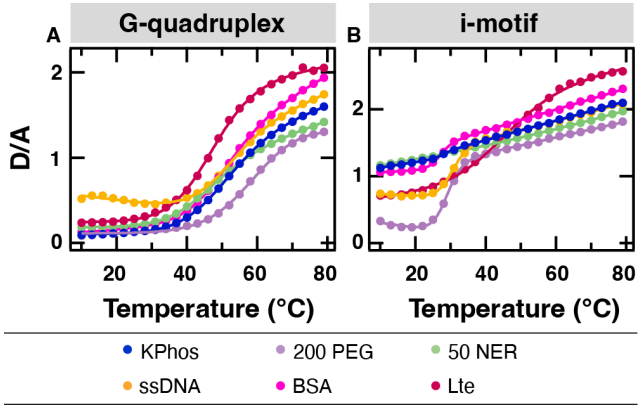

Figure 3. Representative equilibrium temperature denaturation of **(A)** G4 and **(B)** iM monitored by fluorescence spectroscopy excited at 480 nm and collected from 475 to 700 nm. The signal from two-color FRET experiments is reported as a D/A ratio. Experiments were conducted in 10 mM potassium phosphate, 200 mM KCl, 1 mM K_2EDTA, pH 7.0 alone (blue) or with 200 mg/ml PEG (purple), 50% NER (green), 10 mg/ml ssDNA (yellow), or 0.5-1 mg/ml nuclear cell lysate (red).

Lysis buffers have been engineered to maintain the structure and activity of proteins, and therefore likely replicate the

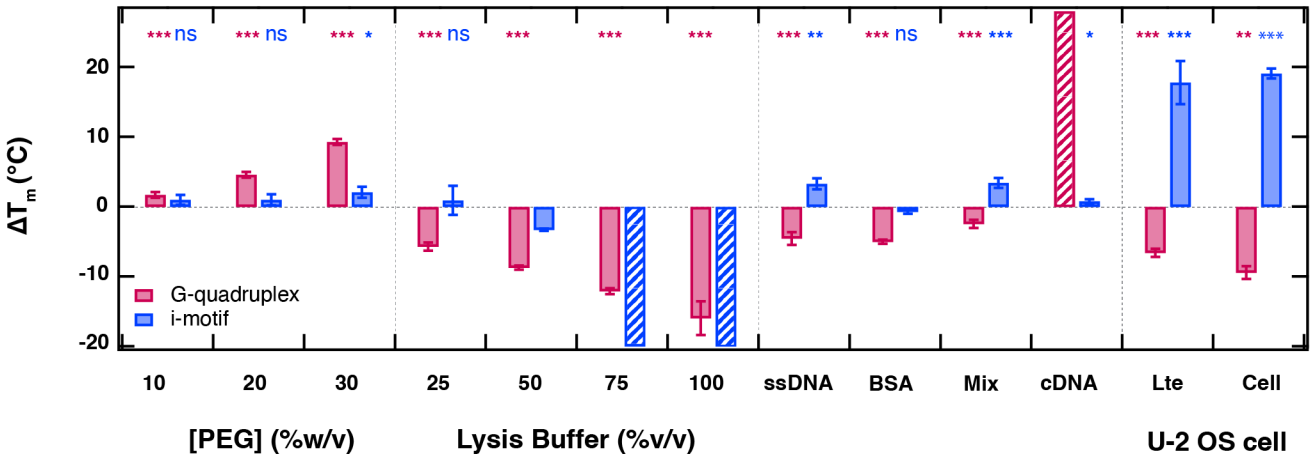

Figure 4. Effect of macromolecular crowding and chemical interactions on the stability of G4 (magenta) and iM (blue). To visualize stability differences, we plotted the change in melting temperature (ΔTm), calculated as the average melting temperature of each test condition minus that of the standard buffer (10 mM potassium phosphate, 200 mM KCl, 1 mM K_2EDTA, pH 7.0). Test conditions included macromolecular crowding (10-30 %w/v PEG10k), cell-mimic chemical interactions including 25–100% (v/v) NER lysis buffer, 10 mg/ml salmon sperm DNA (ssDNA), 0.5 μM complementary DNA (cDNA), 1 mg/mL BSA, and a mixture of 15% w/v PEG10k, 37.5 %(v/v) NER, 2.5 mg/ml ssDNA, and 10 mg/ml BSA in standard buffer (Mix). Also shown are stability differences between standard buffer and U-2 OS nuclear lysate (Lte), and between standard buffer and the nucleus of a living U-2 OS cell (Cell). Bars filled with diagonal stripes are conditions where the stability was too high or low to be confidently fit. Error bars are derived from propagating the standard error of three experiments in phosphate buffer and the standard error of three experiments for each respective condition (one experiment for iM in 50% NER, ≈40 measurements for G-quadruplex, and ≈60 measurements for i-motif in the nucleus of U-2 OS cells). ***p<0.001; ** p<0.01; *p<0.05; ns p>0.05 between control condition (standard buffer) and test condition by a two-tailed t test. Statistical tests were not performed for conditions where the T_m was not quantified or only one measurement is reported.

effects of many non-specific interactions present in cells. Cytosolic and nuclear lysis buffers have been previously used to mimic influences from non-specific interactions in their respective compartments.[40,66–69] In this spirit, we performed experiments in nuclear lysis buffer (NER, ThermoFisher Scientific) to mimic non-specific interactions with ions (≈200 mM NaCl), small organic molecules (PBS, ≈5 mM EDTA), and short-chain fatty acids (≈0.1% Triton X-100) within the nuclei of cells (Patent No. 9580462 B2). We observed a linear trend in destabilization of G4 with increasing concentrations of NER, with 50 %v/v best matching the stability inside the nuclei of U-2 OS cells (Figure 4, Figure S5A). However, NER could not be used to replicate the in-cell stability of iM. Similar to G4, iM is destabilized by NER; At %v/v >50% the i-motif was so destabilized that the melting temperature could not be confidently measured (Figure 4, Figure S5B-C). That the stability of iM in NER is opposite of the nuclear stability suggests that the difference between nuclear and in vitro stability is not due to non-specific interactions with small organic molecules and metabolites.

Repulsions arising from the negatively charged phosphate backbone of DNA are an important factor in the electrostatic interactions that govern the thermodynamic stability of DNA.[68] The repulsive strength of DNA in the nucleus has been found to stabilize RNA secondary structures and, therefore, likely also stabilize DNA secondary structures like G4 and iM.[40,60] To test this, we quantified G4 and iM folding in the presence of 10 mg/ml salmon sperm DNA (ssDNA), a mimic of non-specific electrostatic repulsion with nearby DNA molecules. In ssDNA, G4 is destabilized by ≈5 °C and iM is stabilized by ≈3 °C to 49.8 ± 0.9 °C and 30.8 ± 0.8 °C, respectively (Figure 4, Figure S6, Table S3, Table S5). Since the large opposing stabilities are not reproduced, nonspecific electrostatic interactions with nucleic acids cannot completely explain the opposite stability trends of G4 and iM observed inside cells.

Another source of charge-charge interactions in the nucleus is proteins. Therefore, we also tested the effect of nonspecific chemical interactions from proteins on the stability of G4 and iM using BSA since it is often employed in biochemical assays and highly stable.[70] While BSA destabilized G4 by ≈6 °C, the effect on iM was negligible (Figure 4, Tables S3 and S5). Since iM is stabilized by ≈20 °C inside cells, nonspecific interactions from proteins alone cannot justify the opposite trends.

Perhaps unsurprisingly, no single macromolecular crowding or non-specific chemical effect accounts for the nuclear stabilities of both G4 and iM. Rather, the different effects counteract each other to produce the observed in-cell stabilities. It is well established that the effects of steric crowding and non-steric chemical interactions are nonadditive.[40,66,69] A true nuclear mimetic would produce all of these effects in tandem. To account for crowding and varying chemical effects, we created a mixture with 150 mg/ml PEG10K, 37.5 %v/v NER, 2.5 mg/ml ssDNA, and 10 mg/ml BSA. This results in a ≈3 °C destabilization of G4 and a ≈3 °C

stabilization of iM (Figure 4, Figure S7). Evidently, the combination of crowding, ionic strength, electrostatics, and non-specific interactions with macromolecules cannot yield the magnitude of the opposite stability trends of G4 and iM observed in living cells.

Weak, specific chemical interactions with nuclear proteins reproduce the opposite nuclear stability trends of G4 and iM. Under native conditions the G- and C- rich strands of G4 and iM are present along with their complementary C- and G- rich strands, respectively. It is possible that specific interactions with their complementary strand modulates stability. Therefore, we measured the stability of G4 and iM in vitro in the presence of their complementary DNA (cDNA) strands in a 1:1 ratio at neutral pH. Although i-motif is mildly stabilized, G4 exhibits large D/A values and a decrease in D/A with temperature consistent with the melting of duplex structure (Figure 4, Figure S8).[71–73] Since G4 and iM structures can compete with duplex formation in cells,[11,74] cDNA is likely not the key contributor in the opposing stability trends.

Another possibility is that weak, specific interactions with other macromolecules in the nucleus are the major modulators of G4 and iM stability. Recently, weak interactions from proteins in the nucleus were shown to have a direct effect on DNA G-quadruplexes inside cells.[75] Therefore, we used dilute U-2 OS nuclear cell lysate (Lte) to track the contributions from specific interactions with nuclear proteins to folding. Initial D/A values show that Lte promotes folding of both DNAs (Figure 3, red). Intriguingly, both DNAs access more extended unfolded states than in any other condition tested, suggesting that interactions with proteins promote more extended unfolded states. The stability trends in Lte most closely resemble in-cell data for both G4 and iM (Figure 4, Figure S9). Previous protein folding and binding studies have identified cell lysate as the most accurate mimic for in-cell dynamics.[41,69,76] Because the concentration of proteins in the nuclear cell lysate is a fraction of what is present inside cells, our measurements can reproduce the opposite stability trends but not the absolute melting temperatures of G4 and iM in living U-2 OS cells. Nonetheless, our experiments in nuclear cell lysate show that specific interactions with proteins within the nucleus are the major contributors of the stability of G4 and iM inside cells.

Nuclear proteins cannot account for in-cell folding dynamics. In addition to thermodynamics, we compared the folding dynamics of G4 and iM in vitro and in cells. To extract relaxation lifetimes, we monitored the D/A signal over time for a temperature jump to T_m. The transients were fit to a double exponential function where the first exponential accounts for the instrument response and unresolved dynamics and the second exponential are the DNA dynamics (Equation 2). Our fit includes a stretch factor that provides information about deviations from two-state behavior.

In aqueous buffer, G4 has a relaxation lifetime, τ, of 0.19 ± 0.03 s (n=16) which is in good agreement with previous work.[77] However, folding inside cells is remarkably slow with an increase in τ to 7 ± 1 s (n=17) (Figure 5A). Because G4 was slow to reach equilibrium inside cells, we extended the length of our jumps from 5 seconds to 20 seconds (Figure S10). No significant deviations from two-state behavior were found for measurements in aqueous buffer, which required a β value of 1 to be fitted with high confidence. While the average β value in cells was 1.0 ± 0.1, β ranged from 0.72 to 2.3 deviating far from a single exponential function. This can occur when there are multiple populations with different relaxation lifetimes that are averaged together in an ensemble measurement. β values > 1 may also indicate that the folding mechanism is multi-state inside the cell. Indeed, it is well established that the folding landscape of TBA is more rugged and complex than that of a simple two-state model;[78,79] in vitro, the transitions between local intermediate states occur on the sub-millisecond timescale and cannot be captured by FReI, likely giving rise to the apparent two-state behavior. Our data suggest that the folding of intermediate states is slowed inside cells, that new slow intermediates states are accessed, and/or that there are multiple populations with different relaxation lifetimes.

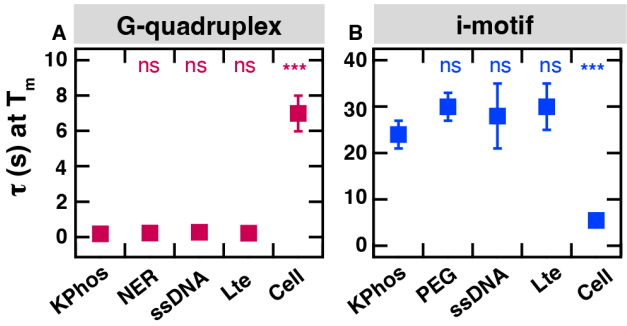

Figure 5. Average relaxation lifetimes (τ) of **(A)** G4 and **(B)** iM following a temperature-jump to T_m in KPhos (10 mM potassium phosphate, 200 mM KCl, 1 mM K_2EDTA, pH 7.0), 200 mg/ml PEG, 50 (%v/v) lysis buffer (NER), 10 mg/ml ssDNA, dilute nuclear cell lysate (Lte), and in the nuclei of fifteen U-2 OS cells. Data was fitted to Equation 2. Data could not be fit for G4 in PEG (too fast) and iM in NER lysis buffer (too small amplitude). Error bars indicate standard error of the mean of three measurements for in vitro conditions and approximately fifteen measurements for cells. ***p<0.001 and ns p>0.05 between experiments (n=3) in standard buffer (KPhos) and each respective condition derived with a two-tailed t test.

While G4 folding is slowed down inside cells, the opposite was observed for iM. Relaxation lifetimes of iM were four times faster inside cells compared to in vitro (Figure 5B). In vitro, the dynamics were so slow that iM required longer t-jumps to achieve equilibrium. Therefore, the length of t-jumps was extended from 10 seconds to 90 seconds to accommodate the slower relaxation lifetimes (Figure S11). Such slow rates have been observed for iM where folding times can range from several minutes to hours.[80,81] In aqueous buffer at neutral pH, the observed relaxation time constant is 24 ± 2 s with a β value of 1.5 ± 0.3. In cells, iM had an average relaxation lifetime of 5.5 ± 0.7 s (n = 14) with a β factor of 3.0 ± 0.5. The in-cell β value ranged from 1 to 7

(Table S4). β values > 1 are consistent with a multi-state mechanism but may also arise from heterogeneity in the population. In fact, like G-quadruplexes, i-motif DNA formation is driven by kinetic partitioning, with the process involving multiple intermediate species.[45,81–83]

To test whether macromolecular crowding or chemical interactions can account for the folding kinetics of G4 and iM inside cells, we performed temperature jumps in PEG, NER, ssDNA, and Lte (Figure 5, Table S6-7). However, none of the relaxation lifetimes measured in these conditions vary significantly from standard phosphate buffer. Despite the good agreement between stabilities in cells and in nuclear cell lysates, the G4/iM in-cell kinetics are not reproduced in nuclear cell lysate alone.

Organization by phase separation is the key contributor of opposing G4 and iM kinetics. Although prior studies confirm the formation of G4/iM puncta in the nuclei of living cells,[29–31,84,85] it is unclear how their dynamics are affected by condensation. Given that the in-cell data revealed β values indicative of multi-state kinetics along with the apparent spatial heterogeneity in the G4/iM populations within the nucleus, we hypothesized that organization by phase separation modulates the folding kinetics of G4 and iM. Not only was nuclear cell lysate the only in vitro condition to match the in-cell thermodynamics, but it was also the only condition that promoted condensation (Figure S12). To examine the impact of phase separation on G4 and iM stability and kinetics further, we induced phase separation with 0.1 mg/ml poly-L-lysine (PLL). PLL is a cationic homopolypeptide that promotes phase separation of negatively charged polymers like DNA.[86] A turbidity assay reveals that phase separation occurs with concentrations as low as 5 μM for both G4 and iM (Figure S13).

Fluorescence imaging confirms that both G4 and iM undergo phase separation into droplets in the presence of PLL (Figure 6A-B). Imaging with unlabeled G4 and iM in the presence of FITC-labeled PLL confirms that PLL is localized in the droplets with the DNA (Figure 6C-D). Interestingly, iM droplets are larger than G4 droplets, likely due to its larger size.[87]. To examine the role of phase separation in the differential stability and kinetic trends of both structures, we performed temperature jumps on the PLL-induced droplets. In 0.1 mg/ml PLL, the relaxation lifetime of G4 was slowed to least 20 s (Figure 6D). Conversely, the relaxation lifetime of iM was sped to an average of 5 ± 2 s (Figure 6E). Thus, measurements in condensates match the kinetic trends.

Associative phase separation induced by attractive interactions between negatively charged DNA and positively charged multivalent cations and proteins is well documented.[88–91] In fact, prior studies of G-quadruplex and i-motif droplets found that LLPS is driven by both electrostatic and hydrophobic π-π stacking interactions between the anionic DNA and the cationic aromatic amino acids.[84,88] Such interactions with proteins can fine tune the stability of these non-canonical structures. There are several G4/iM binding proteins that have been shown to be either destabilizing or stabilizing.[92–100] For example, binding to the positively charged histone H1 tail, in conjunction with condensate formation, promoted the assembly of G-quadruplex and i-motif DNA.[88] Our measurements in both nuclear cell lysate and in living cells exhibit larger unfolded D/A ratios for both G4 and iM compared to that in phosphate buffer. Notably, such large D/A values in the nucleus suggest a more expanded conformation that provides greater accessibility for potential positively charged binding partners to interact and promote condensation and folding. Indeed, prior studies show polymer flexibility and nucleobase accessibility are important for driving more favorable π-π and π-cation interactions to stabilize condensate formation, i.e. rigid complexes involving dsDNA-PLL showed reduced condensate formation compared to more flexible single-stranded DNA.[101,102] Together, our thermodynamic and kinetic results revealed that the stability and kinetics of both G4 and iM structures inside cells are primarily modulated by phase separation due to the interaction with positively charged species.

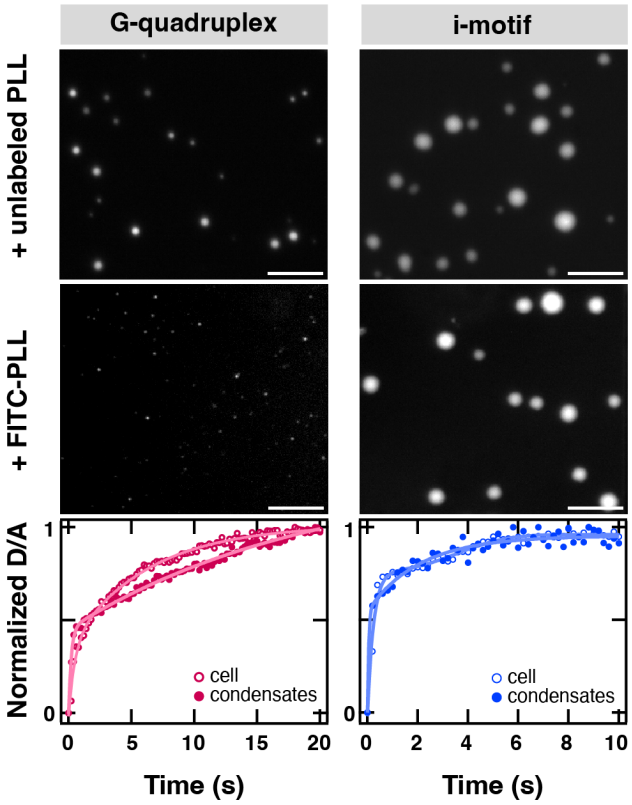

Figure 6. Images of 5 μM FRET-labeled **(A)** G4 and **(B)** iM in the presence of 0.1 mg/ml unlabeled poly-L-lysine (PLL) in phosphate buffer (10 mM potassium phosphate, 200 mM KCl, 1 mM K_2EDTA pH 7.0). Images of 5 μM unlabeled **(C)** G4 and **(D)** iM in the presence of 0.1 mg/ml FITC-labeled PLL in phosphate buffer. Scale bar is 5 μm. Relaxation lifetimes extracted from the condensates containing FRET-labeled **(E)** G4 and **(F)** iM containing 0.1 mg/ml unlabeled PLL in phosphate buffer at pH 7.0.

CONCLUSION

G-quadruplexes and i-motifs have been predominantly studied *in vitro* with only recent evidence confirming the presence of these non-canonical structures inside cells.[28–30,85] However, it remains unclear whether in vitro studies accurately capture their behaviors in the complex cellular environment. To address this gap, we use a combination of in vitro and in-cell FRET measurements to rationalize the stability and dynamics of G4 and iM measured inside living cells. We find that (a) G4 is destabilized by approximately ≈10 °C and iM is stabilized by ≈20 °C inside cells and (b) while G4 folding is slower by two orders of magnitude in cells, iM folding is approximately four times faster. To explain the opposing stability and kinetic trends of G4 and iM in cells, we consider four major factors: macromolecular crowding, nonspecific chemical interactions, specific chemical interactions, and associative phase separation.

Our results demonstrate the importance of studying nucleic acid folding and dynamics in the native cellular environment. The stabilities of G4 and iM are dependent on specific interactions with proteins in the nucleus, and the kinetics are further regulated by phased separation with positively charged species. While future work is necessary to identify the specific DNA-binding proteins that induce phase separation of G4 and iM, our studies suggest that phase separation modulates not just the kinetics of these structures but also the thermodynamics. Both G-quadruplex and i-motif structures are enriched in the promoter regions of the genome, pooled with several transcriptional factors. Together, our results shed light on how the intranuclear environment promotes the formation of functionally relevant structures with kinetics on a timescale for key biological processes and underscores the importance of studying DNA stability and dynamics inside cells. This is especially crucial for biomedical applications where the effectiveness of therapies relies on targeting the correct ensemble of states.

ASSOCIATED CONTENT

Supporting Information

The Supporting Information is available free of charge on the ACS Publications website.

Experimental details and discussion of CD measurements; CD melts, FRET melts, FRET kinetic traces, and turbidity assays; complete DNA sequences; thermodynamic and kinetic fitting parameters for in vitro and in-cell G4/iM FReI measurements (PDF).

AUTHOR INFORMATION

Corresponding Author

* Caitlin M. Davis – Department of Chemistry, Yale University, New Haven, CT 06511, United States; Email: c.davis@yale.edu

Present Addresses

†Physical Sciences Inc., 20 New England Business Center, Andover, MA 01810

Author Contributions

B.P. acquired the data, analyzed the data, and wrote the manuscript. C.H. analyzed the data and edited the manuscript. H.Y. conceived the work, acquired preliminary data, and edited the manuscript. C.M.D. conceived the work, supervised the experiments, analyzed data, and wrote the manuscript. All authors have given approval to the final version of the manuscript.

Notes

The authors declare no competing financial interest.

ACKNOWLEDGMENTS

This work was supported by National Institutes of Health (NIH) grant R35 GM151146. B.P. was partially supported by the NIH under Chemical Biology Training Grant T32 GM067543. C.H. was partially supported by the Yale College Dean's Office through the STARS II Program. This research made use of the Chemical and Biophysical Instrumentation Center at Yale University (RRID:SCR_021738).

REFERENCES

(1) Gehring, K.; Leroy, J.-L.; Guéron, M. A Tetrameric DNA Structure with Protonated Cytosine-Cytosine Base Pairs. *Nature* **1993**, *363* (6429), 561–565. https://doi.org/10.1038/363561a0.

(2) Bochman, M. L.; Paeschke, K.; Zakian, V. A. DNA Secondary Structures: Stability and Function of G-Quadruplex Structures. *Nat Rev Genet* **2012**, *13* (11), 770–780. https://doi.org/10.1038/nrg3296.

(3) Dong, Y.; Yang, Z.; Liu, D. DNA Nanotechnology Based on I-Motif Structures. *Acc Chem Res* **2014**, *47* (6), 1853–1860. https://doi.org/10.1021/ar500073a.

(4) Dong, J.; O'Hagan, M. P.; Willner, I. Switchable and Dynamic G-Quadruplexes and Their Applications. *Chem Soc Rev* **2022**, *51* (17), 7631–7661. https://doi.org/10.1039/d2cs00317a.

(5) Debnath, M.; Fatma, K.; Dash, J. Chemical Regulation of DNA I-Motifs for Nanobiotechnology and Therapeutics. *Angewandte Chemie* **2019**, *131* (10), 2968–2983. https://doi.org/10.1002/ange.201813288.

(6) Li, T.; Famulok, M. I-Motif-Programmed Functionalization of DNA Nanocircles. *J Am Chem Soc* **2013**, *135* (4), 1593–1599. https://doi.org/10.1021/ja3118224.

(7) Hu, Y.; Cecconello, A.; Idili, A.; Ricci, F.; Willner, I. Triplex DNA Nanostructures: From Basic Properties to Applications. *Angew Chem Int Ed Engl* **2017**, *56* (48), 15210–15233. https://doi.org/10.1002/anie.201701868.

(8) Kahn, J. S.; Hu, Y.; Willner, I. Stimuli-Responsive DNA-Based Hydrogels: From Basic Principles to Applications. *Acc Chem Res* **2017**, *50* (4), 680–690. https://doi.org/10.1021/acs.accounts.6b00542.

(9) Brooks, T. A.; Kendrick, S.; Hurley, L. Making Sense of G-Quadruplex and i-Motif Functions in Oncogene Promoters. *FEBS J* **2010**, *277* (17), 3459–3469. https://doi.org/10.1111/j.1742-4658.2010.07759.x.

(10) Ahmed, S.; Kintanar, A.; Henderson, E. Human Telomeric C–Strand Tetraplexes. *Nat Struct Mol Biol* **1994**, *1* (2), 83–88. https://doi.org/10.1038/nsb0294-83.

(11) Xu, Y.; Sugiyama, H. Formation of the G-Quadruplex and i-Motif Structures in Retinoblastoma Susceptibility Genes (Rb). *Nucleic*

Acids Research **2006**, *34* (3), 949–954. https://doi.org/10.1093/nar/gkj485.

(12) Rankin, S.; Reszka, A. P.; Huppert, J.; Zloh, M.; Parkinson, G. N.; Todd, A. K.; Ladame, S.; Balasubramanian, S.; Neidle, S. Putative DNA Quadruplex Formation within the Human C-Kit Oncogene. *J Am Chem Soc* **2005**, *127* (30), 10584–10589. https://doi.org/10.1021/ja050823u.

(13) Li, K. S.; Jordan, D.; Lin, L. Y.; McCarthy, S. E.; Schneekloth, J. S.; Yatsunyk, L. A. Crystal Structure of an I-Motif from the HRAS Oncogene Promoter. *Angew Chem Int Ed Engl* **2023**, *62* (26), e202301666. https://doi.org/10.1002/anie.202301666.

(14) Li, C.; Wang, H.; Yin, Z.; Fang, P.; Xiao, R.; Xiang, Y.; Wang, W.; Li, Q.; Huang, B.; Huang, J.; Liang, K. Ligand-Induced Native G-Quadruplex Stabilization Impairs Transcription Initiation. *Genome Res* **2021**, *31* (9), 1546–1560. https://doi.org/10.1101/gr.275431.121.

(15) Cogoi, S.; Xodo, L. E. G-Quadruplex Formation within the Promoter of the KRAS Proto-Oncogene and Its Effect on Transcription. *Nucleic Acids Res* **2006**, *34* (9), 2536–2549. https://doi.org/10.1093/nar/gkl286.

(16) Sun, D.; Thompson, B.; Cathers, B. E.; Salazar, M.; Kerwin, S. M.; Trent, J. O.; Jenkins, T. C.; Neidle, S.; Hurley, L. H. Inhibition of Human Telomerase by a G-Quadruplex-Interactive Compound. *J. Med. Chem.* **1997**, *40* (14), 2113–2116. https://doi.org/10.1021/jm970199z.

(17) Kendrick, S.; Muranyi, A.; Gokhale, V.; Hurley, L. H.; Rimsza, L. M. Simultaneous Drug Targeting of the Promoter MYC G-Quadruplex and BCL2 i-Motif in Diffuse Large B-Cell Lymphoma Delays Tumor Growth. *J Med Chem* **2017**, *60* (15), 6587–6597. https://doi.org/10.1021/acs.jmedchem.7b00298.

(18) Kang, H.-J.; Kendrick, S.; Hecht, S. M.; Hurley, L. H. The Transcriptional Complex between the BCL2 I-Motif and hnRNP LL Is a Molecular Switch for Control of Gene Expression That Can Be Modulated by Small Molecules. *J Am Chem Soc* **2014**, *136* (11), 4172–4185. https://doi.org/10.1021/ja4109352.

(19) Kaiser, C. E.; Van Ert, N. A.; Agrawal, P.; Chawla, R.; Yang, D.; Hurley, L. H. Insight into the Complexity of the I-Motif and G-Quadruplex DNA Structures Formed in the KRAS Promoter and Subsequent Drug-Induced Gene Repression. *J Am Chem Soc* **2017**, *139* (25), 8522–8536. https://doi.org/10.1021/jacs.7b02046.

(20) Luo, X.; Zhang, J.; Gao, Y.; Pan, W.; Yang, Y.; Li, X.; Chen, L.; Wang, C.; Wang, Y. Emerging Roles of I-Motif in Gene Expression and Disease Treatment. *Front Pharmacol* **2023**, *14*, 1136251. https://doi.org/10.3389/fphar.2023.1136251.

(21) Jana, J.; Weisz, K. Thermodynamic Stability of G-Quadruplexes: Impact of Sequence and Environment. *ChemBioChem* **2021**, *22* (19), 2848–2856. https://doi.org/10.1002/cbic.202100127.

(22) Irving, K. L.; King, J. J.; Waller, Z. A. E.; Evans, C. W.; Smith, N. M. Stability and Context of Intercalated Motifs (i-Motifs) for Biological Applications. *Biochimie* **2022**, *198*, 33–47. https://doi.org/10.1016/j.biochi.2022.03.001.

(23) Leroy, J. L.; Guéron, M.; Mergny, J. L.; Hélène, C. Intramolecular Folding of a Fragment of the Cytosine-Rich Strand of Telomeric DNA into an i-Motif. *Nucleic Acids Res* **1994**, *22* (9), 1600–1606. https://doi.org/10.1093/nar/22.9.1600.

(24) Nonin-Lecomte, S.; Leroy, J. L. Structure of a C-Rich Strand Fragment of the Human Centromeric Satellite III: A pH-Dependent Intercalation Topology1. *Journal of Molecular Biology* **2001**, *309* (2), 491–506. https://doi.org/10.1006/jmbi.2001.4679.

(25) Kaushik, M.; Suehl, N.; Marky, L. A. Calorimetric Unfolding of the Bimolecular and I-Motif Complexes of the Human Telomere Complementary Strand, d(C3TA2)4. *Biophysical Chemistry* **2007**, *126* (1), 154–164. https://doi.org/10.1016/j.bpc.2006.05.031.

(26) Mergny, J.-L.; Lacroix, L. Kinetics and Thermodynamics of I-DNA Formation: Phosphodiester versus Modified Oligodeoxynucleotides. *Nucleic Acids Research* **1998**, *26* (21), 4797–4803. https://doi.org/10.1093/nar/26.21.4797.

(27) Saxena, S.; Joshi, S.; Shankaraswamy, J.; Tyagi, S.; Kukreti, S. Magnesium and Molecular Crowding of the Cosolutes Stabilize the I-Motif Structure at Physiological pH. *Biopolymers* **2017**, *107* (7). https://doi.org/10.1002/bip.23018.

(28) Di Antonio, M.; Ponjavic, A.; Radzevičius, A.; Ranasinghe, R. T.; Catalano, M.; Zhang, X.; Shen, J.; Needham, L.-M.; Lee, S. F.; Klenerman, D.; Balasubramanian, S. Single-Molecule Visualization of DNA G-Quadruplex Formation in Live Cells. *Nat. Chem.* **2020**, *12* (9), 832–837. https://doi.org/10.1038/s41557-020-0506-4.

(29) Summers, P. A.; Lewis, B. W.; Gonzalez-Garcia, J.; Porreca, R. M.; Lim, A. H. M.; Cadinu, P.; Martin-Pintado, N.; Mann, D. J.; Edel, J. B.; Vannier, J. B.; Kuimova, M. K.; Vilar, R. Visualising G-Quadruplex DNA Dynamics in Live Cells by Fluorescence Lifetime Imaging Microscopy. *Nat Commun* **2021**, *12* (1), 162. https://doi.org/10.1038/s41467-020-20414-7.

(30) Zeraati, M.; Langley, D. B.; Schofield, P.; Moye, A. L.; Rouet, R.; Hughes, W. E.; Bryan, T. M.; Dinger, M. E.; Christ, D. I-Motif DNA Structures Are Formed in the Nuclei of Human Cells. *Nature Chem* **2018**, *10* (6), 631–637. https://doi.org/10.1038/s41557-018-0046-3.

(31) Víšková, P.; Ištvánková, E.; Ryneš, J.; Džatko, Š.; Loja, T.; Živković, M. L.; Rigo, R.; El-Khoury, R.; Serrano-Chacón, I.; Damha, M. J.; González, C.; Mergny, J.-L.; Foldynová-Trantírková, S.; Trantírek, L. In-Cell NMR Suggests That DNA i-Motif Levels Are Strongly Depleted in Living Human Cells. *Nat Commun* **2024**, *15* (1), 1992. https://doi.org/10.1038/s41467-024-46221-y.

(32) Kovačič, M.; Podbevšek, P.; Tateishi-Karimata, H.; Takahashi, S.; Sugimoto, N.; Plavec, J. Thrombin Binding Aptamer G-Quadruplex Stabilized by Pyrene-Modified Nucleotides. *Nucleic Acids Res* **2020**, *48* (7), 3975–3986. https://doi.org/10.1093/nar/gkaa118.

(33) Macaya, R. F.; Schultze, P.; Smith, F. W.; Roe, J. A.; Feigon, J. Thrombin-Binding DNA Aptamer Forms a Unimolecular Quadruplex Structure in Solution. *Proc Natl Acad Sci U S A* **1993**, *90* (8), 3745–3749. https://doi.org/10.1073/pnas.90.8.3745.

(34) Avino, A.; Fabrega, C.; Tintore, M.; Eritja, R. Thrombin Binding Aptamer, More than a Simple Aptamer: Chemically Modified Derivatives and Biomedical Applications. *Curr Pharm Des* **2012**, *18* (14), 2036–2047. https://doi.org/10.2174/138161212799958387.

(35) Bock, L. C.; Griffin, L. C.; Latham, J. A.; Vermaas, E. H.; Toole, J. J. Selection of Single-Stranded DNA Molecules That Bind and Inhibit Human Thrombin. *Nature* **1992**, *355* (6360), 564–566. https://doi.org/10.1038/355564a0.

(36) Mergny, J.-L.; Lacroix, L.; Han, X.; Leroy, J.-L.; Helene, C. Intramolecular Folding of Pyrimidine Oligodeoxynucleotides into an I-DNA Motif. *J. Am. Chem. Soc.* **1995**, *117* (35), 8887–8898. https://doi.org/10.1021/ja00140a001.

(37) Choi, J.; Kim, S.; Tachikawa, T.; Fujitsuka, M.; Majima, T. pH-Induced Intramolecular Folding Dynamics of i-Motif DNA. *J. Am. Chem. Soc.* **2011**, *133* (40), 16146–16153. https://doi.org/10.1021/ja2061984.

(38) Dhar, A.; Gruebele, M. Fast Relaxation Imaging in Living Cells. *Curr Protoc Protein Sci* **2011**, *Chapter 28*, Unit28.1. https://doi.org/10.1002/0471140864.ps2801s65.

(39) Knab, E.; Davis, C. M. Chemical Interactions Modulate Λ6-85 Stability in Cells. *Protein Science* **2023**, *32* (7), e4698. https://doi.org/10.1002/pro.4698.

(40) Yoo, H.; Davis, C. M. An in Vitro Cytomimetic of In-Cell RNA Folding. *ChemBioChem* **2022**, *23* (20), e202200406. https://doi.org/10.1002/cbic.202200406.

(41) Davis, C. M.; Gruebele, M. Cellular Sticking Can Strongly Reduce Complex Binding by Speeding Dissociation. *J. Phys. Chem. B* **2021**, *125* (15), 3815–3823. https://doi.org/10.1021/acs.jpcb.1c00950.

(42) Rajendran, A.; Nakano, S.; Sugimoto, N. Molecular Crowding of the Cosolutes Induces an Intramolecular I-Motif Structure of Triplet Repeat DNA Oligomers at Neutral pH. *Chem. Commun.* **2010**, *46* (8), 1299–1301. https://doi.org/10.1039/B922050J.

(43) Dhar, A.; Girdhar, K.; Singh, D.; Gelman, H.; Ebbinghaus, S.; Gruebele, M. Protein Stability and Folding Kinetics in the Nucleus and Endoplasmic Reticulum of Eucaryotic Cells. *Biophys J* **2011**, *101* (2), 421–430. https://doi.org/10.1016/j.bpj.2011.05.071.

(44) Hamm, P.; Helbing, J.; Bredenbeck, J. Stretched versus Compressed Exponential Kinetics in α-Helix Folding. *Chemical Physics* **2006**, *323* (1), 54–65. https://doi.org/10.1016/j.chemphys.2005.08.035.

(45) Gao, B.; Zheng, Y.-T.; Su, A.-M.; Sun, B.; Xi, X.-G.; Hou, X.-M. Remodeling the Conformational Dynamics of I-Motif DNA by Helicases in ATP-Independent Mode at Acidic Environment. *iScience* **2022**, *25* (1), 103575. https://doi.org/10.1016/j.isci.2021.103575.

(46) De Cian, A.; Guittat, L.; Kaiser, M.; Saccà, B.; Amrane, S.; Bourdoncle, A.; Alberti, P.; Teulade-Fichou, M.-P.; Lacroix, L.; Mergny, J.-L. Fluorescence-Based Melting Assays for Studying Quadruplex Ligands. *Methods* **2007**, *42* (2), 183–195. https://doi.org/10.1016/j.ymeth.2006.10.004.

(47) Mergny, J.-L.; Maurizot, J.-C. Fluorescence Resonance Energy Transfer as a Probe for G-Quartet Formation by a Telomeric Repeat. *ChemBioChem* **2001**, *2* (2), 124–132. https://doi.org/10.1002/1439-7633(20010202)2:2<124::AID-CBIC124>3.0.CO;2-L.

(48) Mergny, J. L.; Boutorine, A. S.; Garestier, T.; Belloc, F.; Rougée, M.; Bulychev, N. V.; Koshkin, A. A.; Bourson, J.; Lebedev, A. V.; Valeur, B. Fluorescence Energy Transfer as a Probe for Nucleic Acid Structures and Sequences. *Nucleic Acids Res* **1994**, *22* (6), 920–928. https://doi.org/10.1093/nar/22.6.920.

(49) Hancock, R. Chapter Two - The Crowded Nucleus. In *International Review of Cell and Molecular Biology*; Hancock, R., Jeon, K. W., Eds.; New Models of the Cell Nucleus: Crowding, Entropic Forces, Phase Separation, and Fractals; Academic Press, 2014; Vol. 307, pp 15–26. https://doi.org/10.1016/B978-0-12-800046-5.00002-3.

(50) Benink, H. A.; McDougall, M. G.; Klaubert, D. H.; Los, G. V. Direct pH Measurements by Using Subcellular Targeting of 5(and 6-) Carboxyseminaphthorhodafluor in Mammalian Cells. *BioTechniques* **2009**, *47* (3), 769–774. https://doi.org/10.2144/000113220.

(51) Kamei, Y.; Suzuki, M.; Watanabe, K.; Fujimori, K.; Kawasaki, T.; Deguchi, T.; Yoneda, Y.; Todo, T.; Takagi, S.; Funatsu, T.; Yuba, S. Infrared Laser–Mediated Gene Induction in Targeted Single Cells in Vivo. *Nat Methods* **2009**, *6* (1), 79–81. https://doi.org/10.1038/nmeth.1278.

(52) Ebbinghaus, S.; Dhar, A.; McDonald, J. D.; Gruebele, M. Protein Folding Stability and Dynamics Imaged in a Living Cell. *Nat Methods* **2010**, *7* (4), 319–323. https://doi.org/10.1038/nmeth.1435.

(53) Brylski, O.; Shrestha, P.; Gnutt, P.; Gnutt, D.; Mueller, J. W.; Ebbinghaus, S. Cellular ATP Levels Determine the Stability of a Nucleotide Kinase. *Front Mol Biosci* **2021**, *8*, 790304. https://doi.org/10.3389/fmolb.2021.790304.

(54) Brylski, O.; Shrestha, P.; House, P. J.; Gnutt, P.; Mueller, J. W.; Ebbinghaus, S. Disease-Related Protein Variants of the Highly Conserved Enzyme PAPSS2 Show Marginal Stability and Aggregation in Cells. *Front Mol Biosci* **2022**, *9*, 860387. https://doi.org/10.3389/fmolb.2022.860387.

(55) Guzman, I.; Gelman, H.; Tai, J.; Gruebele, M. The Extracellular Protein VlsE Is Destabilized inside Cells. *J Mol Biol* **2014**, *426* (1), 11–20. https://doi.org/10.1016/j.jmb.2013.08.024.

(56) Gao, M.; Gnutt, D.; Orban, A.; Appel, B.; Righetti, F.; Winter, R.; Narberhaus, F.; Müller, S.; Ebbinghaus, S. RNA Hairpin Folding in the Crowded Cell. *Angew Chem Int Ed Engl* **2016**, *55* (9), 3224–3228. https://doi.org/10.1002/anie.201510847.

(57) Bhattacharyya, D.; Mirihana Arachchilage, G.; Basu, S. Metal Cations in G-Quadruplex Folding and Stability. *Frontiers in Chemistry* **2016**, *4*.

(58) Mergny, J. L.; Phan, A. T.; Lacroix, L. Following G-Quartet Formation by UV-Spectroscopy. *FEBS Lett* **1998**, *435* (1), 74–78. https://doi.org/10.1016/s0014-5793(98)01043-6.

(59) Fulton, A. B. How Crowded Is the Cytoplasm? *Cell* **1982**, *30* (2), 345–347. https://doi.org/10.1016/0092-8674(82)90231-8.

(60) Guigas, G.; Kalla, C.; Weiss, M. The Degree of Macromolecular Crowding in the Cytoplasm and Nucleoplasm of Mammalian Cells Is Conserved. *FEBS Letters* **2007**, *581* (26), 5094–5098. https://doi.org/10.1016/j.febslet.2007.09.054.

(61) Minton, A. P. Excluded Volume as a Determinant of Macromolecular Structure and Reactivity. *Biopolymers* **1981**, *20* (10), 2093–2120. https://doi.org/10.1002/bip.1981.360201006.

(62) Miyoshi, D.; Karimata, H.; Sugimoto, N. Hydration Regulates Thermodynamics of G-Quadruplex Formation under Molecular Crowding Conditions. *J. Am. Chem. Soc.* **2006**, *128* (24), 7957–7963. https://doi.org/10.1021/ja061267m.

(63) Cui, J.; Waltman, P.; Le, V. H.; Lewis, E. A. The Effect of Molecular Crowding on the Stability of Human C-MYC Promoter Sequence I-Motif at Neutral pH. *Molecules* **2013**, *18* (10), 12751–12767. https://doi.org/10.3390/molecules181012751.

(64) Abou Assi, H.; Garavís, M.; González, C.; Damha, M. J. I-Motif DNA: Structural Features and Significance to Cell Biology. *Nucleic Acids Res* **2018**, *46* (16), 8038–8056. https://doi.org/10.1093/nar/gky735.

(65) Ames III, A.; Nesbett, F. B. Intracellular and Extracellular Compartments of Mammalian Central Nervous Tissue. *The Journal of Physiology* **1966**, *184* (1), 215–238. https://doi.org/10.1113/jphysiol.1966.sp007912.

(66) Davis, C. M.; Deutsch, J.; Gruebele, M. An in Vitro Mimic of In-cell Solvation for Protein Folding Studies. *Protein Sci* **2020**, *29* (4), 1060–1068. https://doi.org/10.1002/pro.3833.

(67) Tahir, U.; Davis, C. M. Weak, Specific Chemical Interactions Dictate Barnase Stability in Diverse Cellular Environments. bioRxiv September 27, 2024, p 2024.09.26.615174. https://doi.org/10.1101/2024.09.26.615174.

(68) McConnell, K. J.; Beveridge, D. L. DNA Structure: What's in Charge? *Journal of Molecular Biology* **2000**, *304* (5), 803–820. https://doi.org/10.1006/jmbi.2000.4167.

(69) Davis, C. M.; Gruebele, M. Non-Steric Interactions Predict the Trend and Steric Interactions the Offset of Protein Stability in Cells. *ChemPhysChem* **2018**, *19* (18), 2290–2294. https://doi.org/10.1002/cphc.201800534.

(70) Barone, G.; Giancola, C.; Verdoliva, A. DSC Studies on the Denaturation and Aggregation of Serum Albumins. *Thermochimica Acta* **1992**, *199*, 197–205. https://doi.org/10.1016/0040-6031(92)80263-V.

(71) Roxo, C.; Kotkowiak, W.; Pasternak, A. G-Quadruplex-Forming Aptamers—Characteristics, Applications, and Perspectives. *Molecules* **2019**, *24* (20), 3781. https://doi.org/10.3390/molecules24203781.

(72) *Kinetics of quadruplex to duplex conversion - ScienceDirect*. https://www.sciencedirect.com/science/article/pii/S0300908415003065 (accessed 2024-09-21).

(73) Li, H.; Hai, J.; Zhou, J.; Yuan, G. The Formation and Characteristics of the I-Motif Structure within the Promoter of the c-Myb Proto-Oncogene. *Journal of Photochemistry and Photobiology B: Biology* **2016**, *162*, 625–632. https://doi.org/10.1016/j.jphotobiol.2016.07.035.

(74) König, S. L. B.; Huppert, J. L.; Sigel, R. K. O.; Evans, A. C. Distance-Dependent Duplex DNA Destabilization Proximal to G-Quadruplex/i-Motif Sequences. *Nucleic Acids Res* **2013**, *41* (15), 7453–7461. https://doi.org/10.1093/nar/gkt476.

(75) Yamaoki, Y.; Nagata, T.; Kondo, K.; Sakamoto, T.; Takami, S.; Katahira, M. Shedding Light on the Base-Pair Opening Dynamics of Nucleic Acids in Living Human Cells. *Nat Commun* **2022**, *13* (1), 7143. https://doi.org/10.1038/s41467-022-34822-4.

(76) Phillip, Y.; Kiss, V.; Schreiber, G. Protein-Binding Dynamics Imaged in a Living Cell. *Proceedings of the National Academy of Sciences* **2012**, *109* (5), 1461–1466. https://doi.org/10.1073/pnas.1112171109.

(77) Laouer, K.; Schmid, M.; Wien, F.; Changenet, P.; Hache, F. Folding Dynamics of DNA G-Quadruplexes Probed by Millisecond Temperature Jump Circular Dichroism. *J. Phys. Chem. B* **2021**, *125* (29), 8088–8098. https://doi.org/10.1021/acs.jpcb.1c01993.

(78) Bian, Y.; Song, F.; Cao, Z.; Zhao, L.; Yu, J.; Guo, X.; Wang, J. Fast-Folding Pathways of the Thrombin-Binding Aptamer G-Quadruplex Revealed by a Markov State Model. *Biophysical Journal* **2018**, *114* (7), 1529–1538. https://doi.org/10.1016/j.bpj.2018.02.021.

(79) Yang, C.; Kulkarni, M.; Lim, M.; Pak, Y. In Silico Direct Folding of Thrombin-Binding Aptamer G-Quadruplex at All-Atom Level. *Nucleic Acids Res* **2017**, *45* (22), 12648–12656. https://doi.org/10.1093/nar/gkx1079.

(80) Abdelhamid, M. A. S.; Waller, Z. A. E. Tricky Topology: Persistence of Folded Human Telomeric i-Motif DNA at Ambient Temperature and Neutral pH. *Front Chem* **2020**, *8*, 40. https://doi.org/10.3389/fchem.2020.00040.

(81) Školáková, P.; Gajarský, M.; Palacký, J.; Šubert, D.; Renčiuk, D.; Trantírek, L.; Mergny, J.-L.; Vorlíčková, M. DNA I-Motif Formation at Neutral pH Is Driven by Kinetic Partitioning. *Nucleic Acids Research* **2023**, *51* (6), 2950–2962. https://doi.org/10.1093/nar/gkad119.

(82) Lieblein, A. L.; Buck, J.; Schlepckow, K.; Fürtig, B.; Schwalbe, H. Time-Resolved NMR Spectroscopic Studies of DNA i-Motif Folding Reveal Kinetic Partitioning. *Angew Chem Int Ed Engl* **2012**, *51* (1), 250–253. https://doi.org/10.1002/anie.201104938.

(83) Paul, S.; Hossain, S. S.; Samanta, A. Insights into the Folding Pathway of a C-MYC-Promoter-Based i-Motif DNA in Crowded Environments at the Single-Molecule Level. *J. Phys. Chem. B* **2020**, *124* (5), 763–770. https://doi.org/10.1021/acs.jpcb.9b10633.

(84) Gao, Z.; Yuan, J.; He, X.; Wang, H.; Wang, Y. Phase Separation Modulates the Formation and Stabilities of DNA Guanine Quadruplex. *JACS Au* **2023**, *3* (6), 1650–1657. https://doi.org/10.1021/jacsau.3c00106.

(85) Zhang, S.; Sun, H.; Wang, L.; Liu, Y.; Chen, H.; Li, Q.; Guan, A.; Liu, M.; Tang, Y. Real-Time Monitoring of DNA G-Quadruplexes in Living Cells with a Small-Molecule Fluorescent Probe. *Nucleic Acids Research* **2018**, *46* (15), 7522–7532. https://doi.org/10.1093/nar/gky665.

(86) Vieregg, J. R.; Lueckheide, M.; Marciel, A. B.; Leon, L.; Bologna, A. J.; Rivera, J. R.; Tirrell, M. V. Oligonucleotide–Peptide Complexes: Phase Control by Hybridization. *J. Am. Chem. Soc.* **2018**, *140* (5), 1632–1638. https://doi.org/10.1021/jacs.7b03567.

(87) Agarwal, S.; Osmanovic, D.; Klocke, M. A.; Franco, E. The Growth Rate of DNA Condensate Droplets Increases with the Size of Participating Subunits. *ACS Nano* **2022**, *16* (8), 11842–11851. https://doi.org/10.1021/acsnano.2c00084.

(88) Mimura, M.; Tomita, S.; Shinkai, Y.; Hosokai, T.; Kumeta, H.; Saio, T.; Shiraki, K.; Kurita, R. Quadruplex Folding Promotes the Condensation of Linker Histones and DNAs via Liquid–Liquid Phase Separation. *J. Am. Chem. Soc.* **2021**, *143* (26), 9849–9857. https://doi.org/10.1021/jacs.1c03447.

(89) Mohanty, P.; Kapoor, U.; Sundaravadivelu Devarajan, D.; Phan, T. M.; Rizuan, A.; Mittal, J. Principles Governing the Phase Separation of Multidomain Proteins. *Biochemistry* **2022**, *61* (22), 2443–2455. https://doi.org/10.1021/acs.biochem.2c00210.

(90) Sahoo, B. R.; Kocman, V.; Clark, N.; Myers, N.; Deng, X.; Wong, E. L.; Yang, H. J.; Kotar, A.; Guzman, B. B.; Dominguez, D.; Plavec, J.; Bardwell, J. C. A. Protein G-Quadruplex Interactions and Their Effects on Phase Transitions and Protein Aggregation. *Nucleic Acids Res* **2024**, *52* (8), 4702–4722. https://doi.org/10.1093/nar/gkae229.

(91) Nordenskiöld, L.; Shi, X.; Korolev, N.; Zhao, L.; Zhai, Z.; Lindman, B. Liquid-Liquid Phase Separation (LLPS) in DNA and Chromatin Systems from the Perspective of Colloid Physical Chemistry. *Advances in Colloid and Interface Science* **2024**, *326*, 103133. https://doi.org/10.1016/j.cis.2024.103133.

(92) Tosoni, E.; Frasson, I.; Scalabrin, M.; Perrone, R.; Butovskaya, E.; Nadai, M.; Palù, G.; Fabris, D.; Richter, S. N. Nucleolin Stabilizes G-Quadruplex Structures Folded by the LTR Promoter and Silences HIV-1 Viral Transcription. *Nucleic Acids Res* **2015**, *43* (18), 8884–8897. https://doi.org/10.1093/nar/gkv897.

(93) Brázda, V.; Hároníková, L.; Liao, J. C. C.; Fojta, M. DNA and RNA Quadruplex-Binding Proteins. *Int J Mol Sci* **2014**, *15* (10), 17493–17517. https://doi.org/10.3390/ijms151017493.

(94) Cogoi, S.; Shchekotikhin, A. E.; Xodo, L. E. HRAS Is Silenced by Two Neighboring G-Quadruplexes and Activated by MAZ, a Zinc-Finger Transcription Factor with DNA Unfolding Property. *Nucleic Acids Res* **2014**, *42* (13), 8379–8388. https://doi.org/10.1093/nar/gku574.

(95) Pipier, A.; Devaux, A.; Lavergne, T.; Adrait, A.; Couté, Y.; Britton, S.; Calsou, P.; Riou, J. F.; Defrancq, E.; Gomez, D. Constrained G4 Structures Unveil Topology Specificity of Known and New G4 Binding Proteins. *Sci Rep* **2021**, *11* (1), 13469. https://doi.org/10.1038/s41598-021-92806-8.

(96) Mendoza, O.; Bourdoncle, A.; Boulé, J.-B.; Brosh, R. M.; Mergny, J.-L. G-Quadruplexes and Helicases. *Nucleic Acids Res* **2016**, *44* (5), 1989–2006. https://doi.org/10.1093/nar/gkw079.

(97) Wu, G.; Xing, Z.; Tran, E. J.; Yang, D. DDX5 Helicase Resolves G-Quadruplex and Is Involved in MYC Gene Transcriptional Activation. *Proc Natl Acad Sci U S A* **2019**, *116* (41), 20453–20461. https://doi.org/10.1073/pnas.1909047116.

(98) Wu, W.-Q.; Zhang, X.; Bai, D.; Shan, S.-W.; Guo, L.-J. Mechanistic Insights into Poly(C)-Binding Protein hnRNP K Resolving i-Motif DNA Secondary Structures. *J Biol Chem* **2022**, *298* (12), 102670. https://doi.org/10.1016/j.jbc.2022.102670.

(99) Ban, Y.; Ando, Y.; Terai, Y.; Matsumura, R.; Nakane, K.; Iwai, S.; Sato, S.; Yamamoto, J. Profiling of I-Motif-Binding Proteins Reveals Functional Roles of Nucleolin in Regulation of High-Order DNA Structures. *Nucleic Acids Res* **2024**, *52* (22), 13530–13543. https://doi.org/10.1093/nar/gkae1001.

(100) Roy, B.; Talukder, P.; Kang, H.-J.; Tsuen, S. S.; Alam, M. P.; Hurley, L. H.; Hecht, S. M. Interaction of Individual Structural Domains of hnRNP LL with the BCL2 Promoter I-Motif DNA. *J. Am. Chem. Soc.* **2016**, *138* (34), 10950–10962. https://doi.org/10.1021/jacs.6b05036.

(101) Pokhrel, P.; Jonchhe, S.; Pan, W.; Mao, H. Single-Molecular Dissection of Liquid-Liquid Phase Transitions. *J Am Chem Soc* **2023**, *145* (31), 17143–17150. https://doi.org/10.1021/jacs.3c03812.

(102) Mimura, M.; Tomita, S.; Sugai, H.; Shinkai, Y.; Ishihara, S.; Kurita, R. Uncharged Components of Single-Stranded DNA Modulate Liquid–Liquid Phase Separation With Cationic Linker Histone H1. *Front. Cell Dev. Biol.* **2021**, *9*. https://doi.org/10.3389/fcell.2021.710729.

TOC Figure

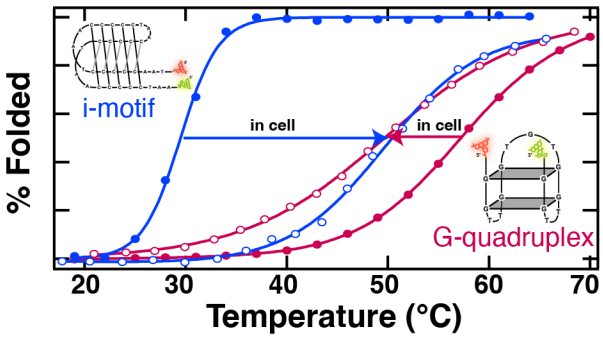
% Folded
i-motif
in cell
in cell
G-quadruplex
20
30
40
50
60
70
Temperature (°C)